Inorganic Chemistry

Article

pubs.acs.org/IC

New Insights into Formation of Trivalent Actinides Complexes with DTPA

Sébastien Leguay,[†] Thomas Vercouter,[§] Sylvain Topin,[‡] Jean Aupiais,[‡] Dominique Guillaumont,[∥] Manuel Miguirditchian,[∥] Philippe Moisy,[∥] and Claire Le Naour*[,†]

[†]CNRS-Université Paris-Sud, IPN 15 rue Georges Clémenceau, 91406 Orsay Cedex, France

[‡]CEA, DAM, DIF, 91297 Arpajon, France

[§]CEA, DEN, DANS, F-91191 Gif-sur-Yvette, France

[∥]CEA, DEN, DRCP, BP 17171, 30207 Bagnols-sur-Cèze, France

Supporting Information

ABSTRACT: Complexation of trivalent actinides with DTPA (diethylenetriamine pentaacetic acid) was studied as a function of pcH and temperature in (Na,H)Cl medium of 0.1 M ionic strength. Formation constants of both complexes $AnHDTPA^{-}$ and $AnDTPA^{2-}$ (where An stands for Am, Cm, and Cf) were determined by TRLFS, CE-ICP-MS, spectrophotometry, and solvent extraction. The values of formation constants obtained from the different techniques are coherent and consistent with reinterpreted literature data, showing a higher stability of Cf complexes than Am and Cm complexes. The effect of temperature indicates that formation constants of protonated and nonprotonated complexes are exothermic with a high positive entropic contribution. DFT calculations were also performed on the An/DTPA system. Geometry optimizations were conducted on $AnDTPA^{2-}$ and $AnHDTPA^{-}$ considering all possible protonation sites. For both complexes, one and two water molecules in the first coordination sphere of curium were also considered. DFT calculations indicate that the lowest energy structures correspond to protonation on oxygen that is not involved in An−DTPA bonds and that the structures with two water molecules are not stable.

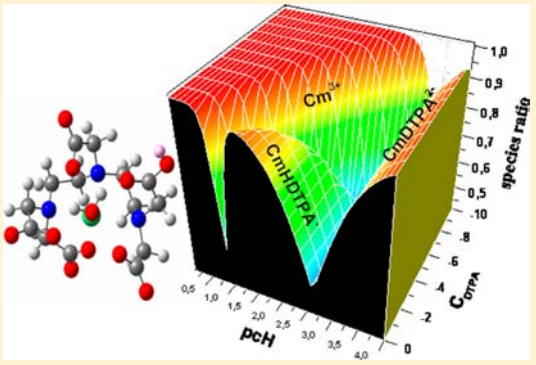

1. INTRODUCTION

Diethylene triamine pentaacetic acid (DTPA) is a complexone of biomedical and environmental interest and also has considerable importance in nuclear industry: DTPA calcium complexes are indeed used for removal of radionuclides from the human body, while this organic acid is an essential reagent in nuclear spent fuel reprocessing processes.[1−3] With five carboxylic and three amino groups this polyaminocarboxylic acid forms stable complexes with almost all metal ions, especially actinides. In the frame of advanced nuclear fuel reprocessing, separation of actinides(III) from lanthanides fission products in order to reduce the radiotoxicity of waste and for transmutation is a major challenge since An(III) and Ln(III) display very close chemical properties. For that purpose, in France, the process SANEX-TODGA (separation of actinides by extraction-*N*,*N*,*N*′,*N*′-tetraoctyl-diglycolamide) was recently developed at CEA to recover the Am and Cm from the fission products in the liquor from the reprocessing of spent nuclear fuel by PUREX process.[4] In the United States, the TALSPEAK process (trivalent actinide−lanthanide separation by phosphorus reagent extraction from aqueous komplexes) has been developed in the 1960s[3] and is still under study.[2] This process is based on selective extraction of lanthanides in organic phase, whereas trivalent americium and curium display higher affinity for the aqueous phase composed of DTPA in lactic acid buffer. To get better insight into the fundamental physicochemical properties of f elements and also improve the TALSPEAK process, the interactions between DTPA and trivalent lanthanides and actinides have been widely investigated. The literature reports especially formation of a 1:1 complex according to the following equilibrium

$$M^{3+} + DTPA^{5-} \Leftrightarrow MDTPA^{2-} \text{ with } \beta_{MDTPA^{2-}} = \frac{[MDTPA^{2-}]}{[M^{3+}][DTPA^{5-}]} \quad (1)$$

The stability constants for these complexes are often higher than 20 in lg units, confirming the strong interaction between DTPA and trivalent elements. The scarce stability constants reported in the literature for $MHDTPA^{-}$ are much lower than those for $MDTPA^{2-}$.[5−7] Moreover, the complex $MHDTPA^{-}$ is only formed in strong acidic media.

More precisely for lanthanides, formation constants of ($LnDTPA^{2-}$, $LnHDTPA^{-}$) as well as the associated enthalpy and entropy variations are available in the literature.[7−10] The

Received: May 25, 2012
Published: November 15, 2012

values of $\lg \beta_{LnDTPA^{2-}}$ increase from La (19.48) to Dy (22.83) with a discontinuity at Gd. For higher lanthanides, formation constants decrease slightly with increasing atomic numbers.[7] The structure of lanthanides/DTPA complexes has also largely been studied in solution as well as in the solid state.[10−15]

Coordination of the lanthanide cation occurs via the five carboxylic oxygen atoms and three nitrogen atoms of DTPA. One water molecule is also involved, leading to a coordination number of nine for the central atom. The corresponding geometry is a distorted capped square antiprism. Recently, DFT calculations performed on the protonated structure Eu-HDTPA$^-$ have confirmed the 9-fold coordination of the lanthanide.[10]

For actinides, the values of stability constants $\beta_{AnDTPA2-}$ determined in the literature are scattered even for studies performed under the same conditions and with the same technique.[5,6,16−23] Reported values are from 22.74[17] to 24.03[16] for $\lg \beta_{AmDTPA^{2-}}$ (Am^{3+}), from 22.38[17] to 23.48[23] for $\lg \beta_{CmDTPA^{2-}}$ (Cm^{3+}), and from 22.57[5] to 24.95[6] for $\lg \beta_{CfDTPA^{2-}}$ (Cf^{3+}). The $\lg \beta_{BkDTPA^{2-}} = 22.79$[5] value is the only one for Bk(III). For plutonium Pu(III), almost all data for $\lg \beta_{PuDTPA^{2-}}$ have been determined by electrochemical measurements in order to avoid oxidation of Pu(III) into Pu(IV) in the presence of DTPA. These experiments have been performed at higher ionic strength (usually I = 1 mol·L^{-1}) and cannot be directly compared to those obtained with the other An(III) at I = 0.1 mol·L^{-1}. No accurate experimental data has been determined for elements lighter than plutonium and heavier than californium. Therefore, it appears to be difficult to extrapolate a trend for the An(III)/DTPA interaction along the actinide series. The works of Baybarz and Brandau are probably the only two studies which allow one to follow the trend of An(III) from the light to the heavy actinides.[5,6] Unfortunately, their conclusions are opposite.

For Baybarz, the $\lg \beta_{AnDTPA^{2-}}$ values increase from Am to Cm and then decrease from Cm to Cf, whereas a continuous increase from Am to Cf is observed by Brandau.

Moreover, in numerous studies, the existence of the protonated complex AnHDTPA$^-$ has been pointed out but not taken into account in the calculation of the formation constants, although experiments were performed at pH lower than 3.[5,16,18−22]

Concerning the temperature effect on formation of AnDTPA^{2-}, only two investigations have been described in the literature.[21,24] Using the calorimetric method in 0.5 M $NaClO_4$ media, the entropy and enthalpy change of AmDTPA^{2-} complex have been determined by Rizkalla et al.:[21] $\Delta H_{AmDTPA^{2-}} = -39.5 \pm 1.0$ kJ·mol^{-1} and $\Delta S_{AmDTPA^{2-}} = 272 \pm 5$ J·K^{-1}·mol^{-1}. Recently, by solvent extraction in concentrated $NaClO_4$ (6.60 M), Choppin et al. evaluated these thermodynamic parameters for americium and curium complexes.[24]

The aim of this work is to establish a complete set of thermodynamical data, including stability constants and enthalpy and entropy variations, and follow the trend of An(III)/DTPA interaction along the actinide series—however limited to three elements over four atomic numbers—in order to improve knowledge on the nature of the interaction: covalent/ionic. For that purpose, the Cm/DTPA system has been first characterized using various techniques, especially time-resolved laser-induced fluorescence spectroscopy (TRLFS). DFT calculations have also been performed to optimize the spatial ligand arrangement for the actinide atom for both complexes: AnDTPA^{2-} and AnHDTPA$^-$. Then we take advantage of the hyphenated technique between capillary electrophoresis and ICP-MS (CE-ICP-MS) to carry out speciation measurements on Am, Cm, and Cf at tracer scale simultaneously, providing accurate relative formation data. The formation constant of the protonated species has also been deduced from UV spectrophotometry experiments with Am and solvent extraction experiments with Am and Cf.

2. EXPERIMENTAL SECTION

2.1. pH Measurement and Free Proton Concentration. The pH meter (781 Metrohm) was calibrated with standard NIST buffers (pH 1.679, 4.005, and 7.000). It was assumed that the junction potentials of saturated KCl/buffer solutions and saturated KCl/samples are identical (I = 0.1 M). The quantity of protons measured in activity was converted to free proton molar concentration (pcH) using the value of the activity coefficient determined by Capone et al. (γ_{H+} = 0.839 ± 0.006).[25] This conversion was necessary since all other species amounts were expressed in molar concentration as well as the acidity constants of DTPA available in the literature.

2.2. Time-Resolved Laser-Induced Fluorescence Spectroscopy (TRLFS). Excitation of Cm(III) was performed at 395−400.2 nm using a quadrupled (266 nm) Nd:YAG laser (Brilliant, Quantel) coupled to an optical parametric oscillator (OPOTEK), providing about 1 mJ with a 10 Hz repetition rate. The laser beam was driven to the quartz cell placed in a glovebox. Emission spectra of the Cm(III) samples were recorded using a polychromator equipped with a 600 mm^{-1} grating (Roper Scientific) and a time-gated intensified CCD camera (PIMAX, Princeton Instruments) as detailed elsewhere.[26] The resolution of the spectra is estimated to be 0.2 nm. Fluorescence spectra were recorded with constant gate delay (1 μs) and gate width (300 μs). Fluorescence lifetimes were derived from the decay of the intensity measured by varying the gate delay for a constant gate width (30 μs).

Electrolytes were prepared by diluting DTPA solution in a HCl/NaCl mixture of 0.1 M ionic strength, as described in the Supporting Information. Aliquots of ^{248}Cm solution (10^{-7} M in 0.1 M HCl) were added to 1.5 mL of each electrolyte, and the pcH was checked systematically (and adjusted when necessary).

2.3. CE-ICP-MS. A commercial Beckman Coulter P/ACE MDQ capillary electrophoresis system (Fullerton, USA) equipped with a UV detection mode was used for all separations in the same conditions that have been recently described (fused silica, 50 μm internal diameter, ∼60 cm lengths, 10.1 cm optical window).[27] An Axiom (VG Elemental, Winsford, Cheshire, U.K.) inductively coupled plasma sector field mass spectrometer (ICP-SF-MS) was coupled with the capillary electrophoresis using a commercial interface (Mira Mist CE, Burgener, Mississauga, Canada).[27] A makeup liquid is introduced thanks to a syringe pump (11 Pico Plus, Harvard Apparatus, Holliston, MA) at a nominal flow rate of 6 μL.min^{-1}. Separations were performed at +10 kV, 25 ± 2 °C and a constant pressure of 0.8 psi (to avoid capillary clogging). The voltage value was chosen with respect to the Ohm law. The buffer vial was changed every run to avoid the effects of electrolysis. Before each run, the capillary was washed with the background electrolyte (BGE) for 10 min at 20 psi and 2 min at 40 psi. Separations were achieved within 25 min. Sample injections were hydrodynamically carried out at 1 psi for 4 s. Under our experimental conditions the temperature excess has been determined as ΔT = 2 °C between the center of the capillary and the liquid coolant. The temperature is therefore considered as homogeneous across the capillary with a ±2 °C confidence in all experiments.

Background electrolytes were prepared by dissolving DTPA in 0.1 M (Na,H) Cl medium for 2 values of pcH (1.42 and 1.92). Then aliquots of ^{248}Cm, ^{243}Am, and ^{249}Cf solutions in 0.1 M HCl and of DMF (marker for electro-osmotic migration) were added to each BGE sample. More details are given in the Supporting Information.

2.4. Solvent Extraction. Organic phases (HDEHP, bis(2-ethylhexyl)phosphoric acid, in TPH, tetrapropene) were preequilibrated with 0.1 M NaCl at pcH = 1.42 in the presence of ^{249}Cf and

dx.doi.org/10.1021/ic3011019 | Inorg. Chem. 2012, 51, 12638−12649

Table 1. Used Acidity Constants of DTPA

	pKa_7	pKa_6	pKa_5	pKa_4	pKa_3	pKa_2	pKa_1
ΔH (kJ·mol^{-1})	no data	no data	no data	no data	6.23 ± 2.93[a]	20.33 ± 2.93[a]	22.76 ± 1.76[a]
T (°C) = 10[d]	1.45 ± 0.15	1.60 ± 0.15	1.80 ± 0.05	2.55 ± 0.05	4.37 ± 0.03	8.73 ± 0.03	10.72 ± 0.02
T (°C) = 20[a]			1.80 ± 0.05	2.55 ± 0.05	4.33	8.6	10.58
T (°C) = 25[d]	1.45 ± 0.15[b]	1.60 ± 0.15[c]	1.80 ± 0.05	2.55 ± 0.05	4.31 ± 0.02	8.54 ± 0.02	10.51 ± 0.01
T (°C) = 50[d]	1.45 ± 0.15	1.60 ± 0.15	1.80 ± 0.05	2.55 ± 0.05	4.23 ± 0.09	8.26 ± 0.09	10.2 ± 0.06

[a]Moeller and Thompson.[7] [b]Lekteman et al.[36] [c]Lekteman et al. and Mentasti et al.[35,36] average. [d]Corrected using the available enthalpy variation from Moeller and Thompson.[7]

^{241}Am and contacted for 60 min with aqueous solution of DTPA in (Na,H)Cl solution of pcH = 1.42. After phase separation, an equal volume of organic and aqueous phase was analyzed by gamma spectrometry. For each isotope, the distribution ratio D was determined by calculating the ratio between the activity in organic and aqueous phase. The uncertainty in D measurements was estimated to be within 10%. More details can be found in the Supporting Information.

2.5. Quantum Chemistry Calculations. The geometries of Am(III), Cm(III), and Cf(III) with DTPA and HDTPA were optimized at the DFT level of theory with the Gaussian 03 program package.[28] Solvation effects were taken into account using an implicit solvation model where the solute is embedded in a molecular-shaped cavity surrounded by a dielectric medium. The integral equation formalism polarizable continuum model (IEFPCM) was used, and the molecular cavity was built up by the UAHF model as implemented in Gaussian 03.

For actinide atoms small-core relativistic effective core potentials developed in the Stuttgart/Cologne group were used together with the accompanying basis set to describe the valence electron density. Small-core RECPs replace 60 core electrons, and the corresponding valence basis sets is (14s13p10d8f) contracted to [10s9p5d4f].[29] For other atoms, the 6-31G* basis set was used. The B3LYP functional was employed.[30,31]

To ensure that minima on the potential-energy surface have been located, analytical vibrational frequencies have been calculated for the optimized structures of Cm complexes. For An(DTPA)$^{2-}$ complexes, X-ray coordinates obtained for a lanthanide complex were used as the starting structure.[32]

3. RESULTS AND DISCUSSION

3.1. Definition of Constants. All formation constants are expressed in terms of equilibrium concentrations and not of ion activities following the recommendations of OECD-NEA expert groups.[33] Thus, the formation constants of $AnH_nDTPA^{(5-n)-}$, $\beta_{i,n}$, are apparent constants that depend on the ionic medium (nature and concentration of the background electrolyte). Each one is described by equilibrium 2 and written according to eq 3

$$An^{3+} + H_iDTPA^{(5-i)-} \Leftrightarrow AnH_nDTPA^{(2-n)-} + (i-n)H^+ \quad (2)$$

$$\beta_{i,n} = \frac{[AnH_nDTPA^{(2-n)-}][H^+]^{i-n}}{[An^{3+}][H_iDTPA^{(5-i)-}]} \quad (3)$$

where i refers to the number of protons involved in the free species of DTPA and n to the number of exchangeable protons in the complex. An overall conditional formation constant is defined by β^{cond} in order to relate the concentration of complexed and uncomplexed An(III) with the total concentration of DTPA, C_{DTPA}. This conditional formation constant formally corresponds to equilibrium 4

$$An(III) + DTPA \overset{\beta^{cond}}{\Longleftrightarrow} An(III)/DTPA \quad (4)$$

and depends on experimental parameters, namely, on pcH. This conditional constant will be directly measured from experimental data and can be related to formation constants, $\beta_{i,n}$.

The individual formation constant $\beta_{i,n}$ can be deduced from β^{cond} by relation 5

$$\beta_{i,n} = \alpha_{H_iDTPA^{(5-i)-}} \times \beta^{cond} \times [H^+]^{i-n} = \beta_{i,n}^{cond} \times [H^+]^{i-n} \quad (5)$$

where $\alpha_{H_iDTPA^{(5-i)-}}$ is defined as

$$\alpha_{H_iDTPA^{(5-i)-}} = \frac{C_{DTPA}}{[H_iDTPA^{(5-i)-}]} \quad (6)$$

Finally, eq 5 can be written in a logarithmic form

$$\lg \beta_{i,n}^{cond} = \lg \beta_{i,n} + (i-n)pcH \quad (7)$$

The values of $\alpha_{H_iDTPA^{(5-i)-}}$ are calculated using eq 8

$$\alpha_{H_iDTPA^{(5-i)-}} = 1 + \sum_{j=1}^{i} (10^{-\sum_{m=j}^{i} pKa_m} \times [H^+]^{j-(i+1)}) + \sum_{j=i+1}^{7} (10^{\sum_{m=i+1}^{j} pKa_m} \times [H^+]^{j-i}) \quad (8)$$

and acidity constants of DTPA from Ka_1 to Ka_7 that are relative to equilibrium 9

$$H_iDTPA^{(5-i)-/or(i-5)+} \Leftrightarrow H_{(i-1)}DTPA^{(4-i)-/or(i-4)+} + H^+ Ka_i = \frac{[H_{(i-1)}DTPA^{(4-i)-}]\cdot[H^+]}{[H_iDTPA^{(5-i)-}]} \quad (9)$$

Literature data of thermodynamic formation constants of complexes can be compared only when Ka_i used for interpretation of experimental data are clearly stated; otherwise, inherent bias may exist. In this work, we used the acidity constants Ka_1–Ka_5 from Moeller and Thompson's work performed at 20 °C and I = 0.1 M (K,H)NO_3.[7] Although a different background electrolyte was used in the present work, effects on Ka_i values of DTPA can be neglected at such low ionic strength. In the case of EDTA indeed, no effect of the anion (Cl^-, NO_3^-) is observed for I = 0.1 M and the difference does not exceed 0.04 lg units between K^+- and Na^+-based electrolyte.[34] The temperature effect on values of Ka_1, Ka_2, and Ka_3 has also been studied by some authors to determine the enthalpy variation of the acid–base reactions. Ka_6 and Ka_7 values are taken from Mentasti et al. and Letkeman et al. at 25 °C and I = 0.1 M.[35,36] For Ka_4–Ka_7 no value of enthalpy variations are reported in the literature. Consequently, these constants have been fixed to their values given at 20–25 °C

dx.doi.org/10.1021/ic3011019 | Inorg. Chem. 2012, 51, 12638–12649

because the corresponding enthalpy variation can be expected to be small regarding the decrease of enthalpy variation along the Ka_i series. Their relative uncertainties have been extended to 0.05 in lg units. All values are listed in Table 1.

3.2. Cm/DTPA System. *3.2.1. Thermodynamic Investigation.* The fluorescence emission spectra of Cm(III) were measured at 25 °C at constant pcH (1.42, 1.92, 2.18, 2.62, and 2.72) and ionic strength (0.1 M NaCl) while increasing DTPA concentrations. Measurements were also performed at 10 and 50 °C for 2 pcH values (1.42 and 2.72). The emission spectrum of Cm^{3+} aquo ion displays a broad band at 594 nm with a fluorescence lifetime of 62 μs (Figure 1). The intensity of this band decreases as DTPA concentration increases; four peaks at 582, 590, 601, and 608 nm show up, in agreement with the four components of the ligand-field split $^6D_{7/2}$ state to the fundamental $^8S_{7/2}$ as mentioned by Beitz, attributed to a $CmDTPA^{2-}$ complex.[37]

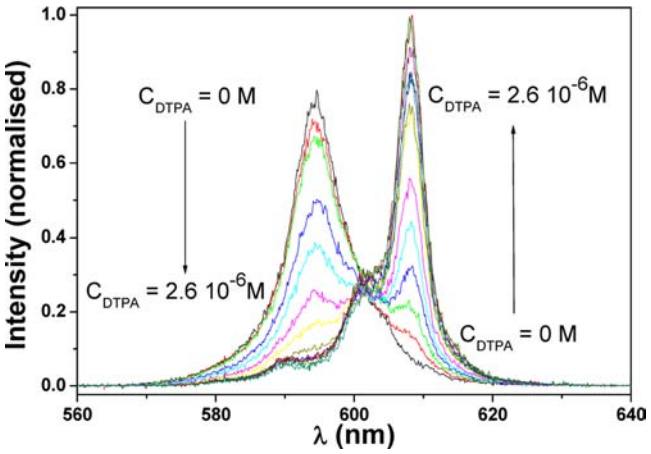

Figure 1. Normalized fluorescence emission spectra of nanomolar Cm(III) solution at various DTPA concentrations in (Na,H)Cl 0.1 M media pcH = 2.72 and T = 25 °C (excitation wavelength 398.2 nm).

The Cm:DTPA ratio in the complex was verified to equal 1 by classical slope analysis of the data at constant pcH (Figure S1, Supporting Information). By examining the spectra from each titration series, the intensity measured at about 600 nm appears to be invariant according to experimental uncertainties, i.e., appears to be an isosbestic point, which would be consistent with formation of a unique 1:1 Cm/DTPA complex. Hence, this spectrum formed along the titration experiment has been attributed to $CmH_nDTPA^{(2-n)-}$ species. Thus, the n value must be determined using data sets at different pcH values.

Each conditional complex formation constant was deduced from the variations of the intensity of the peak measured at 608.1 nm with DTPA concentration. The fluorescence intensity results from emission of a mixture of curium species, Cm^{3+}, and the Cm/DTPA complex and can therefore be expressed as

$$\frac{I(\lambda)}{[\mathrm{Cm}]_{\mathrm{total}}} = x_{\mathrm{Cm}^{3+}} \times I_{\mathrm{Cm}^{3+}}(\lambda) + x_{\mathrm{Cm/DTPA}} \times I_{\mathrm{Cm/DTPA}}(\lambda) \quad (10)$$

where $I(\lambda)$ is the measured fluorescence intensity at the wavelength λ, $I_{species}$ is the fluorescence intensity of the species at λ, and $x_{species}$ is the molar ratio of the species.

Using eqs 5−6, eq 10 is rewritten to express the conditional formation constant, β^{cond}.

Table 2. Conditional Data Obtained with Different Experimental Techniques in This Work and From Reinterpretation of Literature Raw Data (I = 0.1 M and T = 25 °C)

pcH	lg β^{cond}	lg $\alpha_{H_4DTPA^-}$	lg($\beta^{cond} \times \alpha_{H_4DTPA^-}$)	method	ref
1.42	3.00 ± 0.15	1.04	4.0 ± 0.2	TRLFS	this work
1.92	5.25 ± 0.15	0.39	5.6 ± 0.2		
2.18	6.04 ± 0.30	0.30	6.3 ± 0.3		
2.62	7.30 ± 0.15	0.37	7.7 ± 0.2		
2.72	7.73 ± 0.15	0.42	8.2 ± 0.2		
1.42	2.93 ± 0.15	1.04	4.0 ± 0.2	CE-ICP-MS	this work
1.92	5.32 ± 0.30	0.39	5.7 ± 0.3		
2.12	5.44	0.31	5.75	ion exchange	5
2.27	6.03	0.29	6.32		
2.42	6.61	0.31	6.92		
2.72	7.69	0.42	8.11		
1.83	4.59	0.46	5.05	ion exchange	23
1.93	5.10	0.39	5.49		
2.03	5.33	0.37	5.70		
2.10	5.59	0.31	5.90		
2.21	5.96	0.29	6.25		
2.29	6.27	0.29	6.56		
2.47	6.96	0.32	7.28		
2.59	7.40	0.36	7.78		
2.67	7.80	0.40	8.20		
2.78	8.21	0.46	8.67		
1.43	2.98	1.02	4.0	migration	17
1.52	3.28	0.82	4.14		
1.63	3.78	0.69	4.47		
1.72	4.19	0.57	4.76		
1.84	4.64	0.46	5.09		

dx.doi.org/10.1021/ic3011019 | Inorg. Chem. 2012, 51, 12638−12649

$$I(\lambda) = \frac{I_{Cm^{3+}}(\lambda) + I_{Cm/DTPA}(\lambda) \times \beta^{cond} \times C_{DTPA}}{1 + \beta^{cond} \times C_{DTPA}} \quad (11)$$

Equation 11 is eventually used to fit $I(\lambda)$ to the measured fluorescence intensity by adjusting $I_{Cm/DTPA}(\lambda)$ and β^{cond}.

Under some pcH conditions, $I^0_{Cm/DTPA}(\lambda)$ is experimentally determined when the spectra remain constant as the DTPA concentration increases. Otherwise, it should be fitted.

The β^{cond} values are then used in eq 5. The value of i can be chosen at convenience in order to plot the data. In our case, i = 4 is preferable because H_4DTPA^- is a major species in our pcH range, and then it minimizes the uncertainties resulting from propagation of uncertainties of pKa_i in the calculation of $\alpha_{H_4DTPA^-}$.

$$\alpha_{H_4DTPA^-} = 1 + 10^{-pKa1-pKa2-pKa3-pKa4}[H^+]^{-4} + 10^{-pKa2-pKa3-pKa4}[H^+]^{-3} + 10^{-pKa3-pKa4}[H^+]^{-2} + 10^{-pKa4}[H^+]^{-1} + 10^{pKa5}[H^+] + 10^{pKa5+pKa6}[H^+]^2 + 10^{pKa5+pKa6+pKa7}[H^+]^3 \quad (12)$$

The values of $\log \beta^{cond}_{4,n}$ are calculated with the TRLFS and CE-ICP-MS data as well as with raw data from previous studies when available.[5,17,23] These values for Cm(III) are listed in Table 2. The values determined in this work compare well with those recalculated from other raw data for similar pcH values. This supports the fact that measurements performed with different techniques are consistent. As expected, the conditional constant increases as pcH increases, resulting from deprotonation of DTPA molecules.

The variations of $\lg(\beta^{cond} \times \alpha_{H_4DTPA^-})$ as a function of pcH are presented in Figure 2. According to eq 7, the slope of the straight line is $(4 - n)$, where n is the number of H atoms in the complex. The fit of the five values at different pcH deduced from TRLFS experiments gives $(4 - n)$ = 3.2 (n = 0.8). This interpretation is considered not satisfactory because n must be an integer.

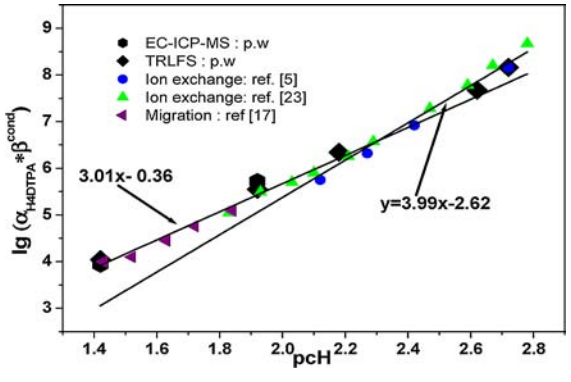

Figure 2. Variation of $\lg(\beta^{cond}\alpha_{H4DTPA})$ as a function of pcH (in 0.1 M media at 25 °C with different methods).

However, the fit performed on the first 3 values (pcH 1.32, 1.92, and 2.18) gives $(4 - n)$ = 3.0 (n = 1.0). On the other hand, the fit of data at pcH 2.18, 2.62, and 2.72 gives $(4 - n)$ = 3.4 (n = 0.6). When the data obtained with CE-ICP-MS (pcH = 1.42, 1.92) and the values originated from literature studies are added, a clear change in slope can be observed in Figure 2 at pcH ≈ 2.4. This can be related to a change in the protonation state of the Cm/DTPA complex. For pcH lower and higher than 2.4, the slopes are 3 (n = 1) and 4 (n = 0), respectively. At pcH lower than 2.4, the protonated complex $CmHDTPA^-$ is the predominant species; at pcH higher than 2.4, complex $CmDTPA^{2-}$ becomes predominant. In view of the pcH range investigated (Table 2), both complexes coexist and have to be considered in determination of apparent formation constants. Neglecting the protonated species at low pcH may interfere with calculation of $AnDTPA^{2-}$ formation constant.[5,16,18,19] For example, the value of apparent formation constants of $AmDTPA^{2-}$ ($\beta_{1,0}$ according to eq 2) in NH_4ClO_4 0.1 M was found to be equal to 24.03 at 0.62 < pcH < 1.52 and 22.92 at 2.08 < pcH < 2.68.[5,16] It seems that assumptions about the protonation state of the complex made in previous studies have led to apparent inconsistencies. The data, as presented here, show on the contrary that the experimental data are consistent.

Moreover, considering $\beta^{cond}\alpha_{H_4DTPA^-}$ as the sum of $\beta^{cond}_{4,1}$ and $\beta^{cond}_{4,0}$ (eq 5), the whole data can be fitted together (eq 13) as shown in Figure S2, Supporting Information

$$\lg(\beta^{cond} \times \alpha_{H_4DTPA^-}) = \frac{\beta_{4,1}}{[H^+]^3} + \frac{\beta_{4,0}}{[H^+]^4} \quad (13)$$

The fit of data obtained in this work gives $\lg \beta_{4,0} = -2.9 \pm 0.18$ and $\lg \beta_{4,1} = -0.35 \pm 0.23$, and the fit of all data gives $\lg \beta_{4,0} = -2.82 \pm 0.05$ and $\lg \beta_{4,1} = -0.46 \pm 0.53$. Our results are therefore in agreement with previous studies.

In the present work, the apparent formation constants of $CmHDTPA^-$ and $CmDTPA^{2-}$ complexes related to equilibria 14 and 15 have been calculated using eq 16.

$$An^{3+} + DTPA^{5-} \Leftrightarrow AnDTPA^{2-} \quad \beta_{0,0} = \frac{[AnDTPA^{2-}]}{[An^{3+}][DTPA^{5-}]} \quad (14)$$

$$An^{3+} + DTPA^{5-} + H^+ \Leftrightarrow AnHDTPA^- \quad \beta_{0,1} = \frac{[AnHDTPA^-]}{[An^{3+}][DTPA^{5-}][H^+]} \quad (15)$$

$$\lg \beta_{0,n} = \lg \beta_{4,n} + pKa_1 + pKa_2 + pKa_3 + pKa_4 \quad (16)$$

The acidity constant of the complex (K_H) is calculated by eq 17

$$AnDTPA^- + H^+ \Leftrightarrow AnHDTPA^- \quad K_H = \frac{\beta_{0,1}}{\beta_{0,0}} \quad (17)$$

Finally, the formation constants have been determined to be 23.0 ± 0.3 for $CmDTPA^{2-}$, 25.6 ± 0.3 for $CmHDTPA^-$, and 2.6 ± 0.6 for K_H (in logarithm).

It should be noticed that the amount of chloride complexes formed in solution has been neglected; less than 4% of chloride complexes should have formed according to the OECD-NEA data.[38]

3.2.2. Temperature Effect. TRLFS experiments were performed at 10, 25, and 50 °C for 2 pcH values: pcH = 1.42 and 2.72 where $CmHDTPA^-$ and $CmDTPA^{2-}$, respectively, are predominant. The enthalpy change induced by variations of acidity constants of DTPA with temperature have been taken into account in the calculation of $\alpha_{DTPA^{5-}}$ (eqs 5 and 8 and Table 1). Results in Table 3 tend to indicate a slight increase of the conditional formation constant with

dx.doi.org/10.1021/ic3011019 | Inorg. Chem. 2012, 51, 12638−12649

Table 3. Formation Constants of Cm/DTPA Complexes at Various pcH and Temperatures in 0.1 M (Na,H)Cl

pcH	T (°C)	$\lg \beta^{cond}$	$\lg \alpha_{DTPA^{5-}}$	$\lg(\lg \alpha_{DTPA^{5-}} \times \lg \beta^{cond})$
1.42	10.0	2.9 ± 0.2	21.7 ± 0.4	24.6 ± 0.6
	25.0	3.0 ± 0.2	21.3 ± 0.2	24.3 ± 0.4
	50.0	3.2 ± 0.2	20.6 ± 0.5	23.8 ± 0.7
2.64	10.0	7.1 ± 0.2	16.2 ± 0.4	23.3 ± 0.6
2.72	25.0	7.7 ± 0.3	15.4 ± 0.2	23.1 ± 0.5
2.72	50.0	7.6 ± 0.3	14.78 ± 0.3	22.4 ± 0.6

increasing temperature, corresponding to a slight decrease when variation of acidity constants of DTPA have been taken into account ($\alpha_{DTPA^{5-}}$ variation with temperature).

The variations of apparent constants as a function of $1/T$ are plotted in Figure 3 and fitted with the Van't Hoff equation, eq

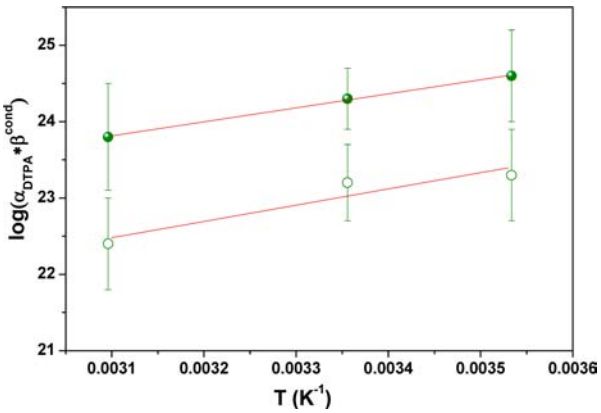

Figure 3. Variations of Cm/DTPA apparent formation constant as a function of $1/T$: at pcH 1.42 (solid circles) and 2.72 (open circles), and linear regression following Van't Hoff law (red straight line).

18, for both pcH values, neglecting the variation of enthalpy with temperature

$$\lg \beta = -\frac{\Delta H(T^0)}{RT \ln 10} + \frac{\Delta S(T^0)}{R \ln 10} \quad (18)$$

where R is the gas constant and T^0 the reference temperature (298.15 K).

Enthalpy variations were found to be equal to −36 ± 3 kJ·mol^{-1} at pcH = 1.42 and −40 ± 13 kJ·mol^{-1} at pcH = 2.72. These values are not significantly different considering the rather large uncertainties with this method, although proportions of each complex are different. Therefore, the enthalpy variations have been assumed to be equal to 38 ± 13 kJ·mol^{-1} for both complexation reactions (eqs 14 and 15). This approximation is supported by the recent results of Tian et al., who obtained a difference of about 5 kJ mol^{-1} between enthalpy variations relative to formation of protonated and nonprotonated Nd and Eu complexes.[10]

Then entropy variations have been calculated according to

$$\Delta G = -RT \ln \beta = \Delta H - T\Delta S \quad (19)$$

Thermodynamic parameters relative to complexation of An(III) with DTPA are listed in Table 4 with the unique data set available in the literature for Am(III). Our results are consistent with those of Rizkalla et al., although experimental conditions are different.[21] Values in Table 4 indicate that the complexes are very stable and their formation is exothermic. Enthalpy of reaction 2 can be considered as the summation of reagents desolvation energy and energy required to form cation−ligand bonds. In the reaction of An^{3+} with $HDTPA^{4-}$or $DTPA^{5-}$, the binding energy in the complex overcomes the dehydration one, leading to favorable enthalpy. The loss of entropy due to formation of the well-ordered chelate An(III)/DTPA complex is counterbalanced by the entropic gain due to disruption of the hydration sphere around reactants (cation and ligand).

3.3. An(III)/DTPA Formation Constant. The formation constants of An(III)/DTPA complexes involving Am and Cf have been determined by solvent extraction and UV−vis spectroscopy in a pcH range where the protonated species is predominant. Then CE-ICP-MS experiments have been performed with the three actinides Am, Cm, and Cf simultaneously.

3.3.1. Solvent Extraction and Spectrophotometry. Solvent extraction experiments were performed with Am and Cf at tracer scale using HDEHP diluted in TPH as organic phase. Distribution ratios D were determined for both elements simultaneously as a function of C_{DTPA} at constant pcH (1.42), temperature (25 °C), and ionic strength ((Na,H)Cl 0.1 M). The variations of D depicted in Figure 4 illustrate formation of

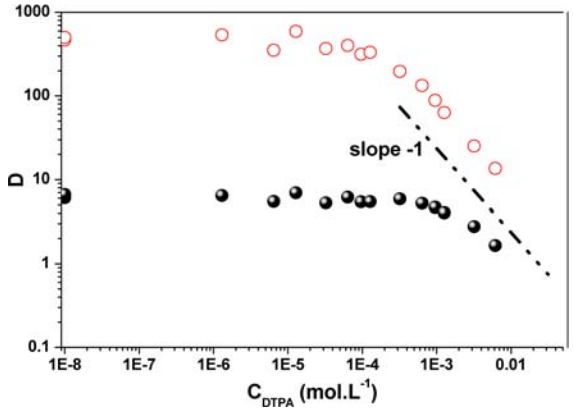

Figure 4. Distribution of Cf^{3+} (red open circle) and Am^{3+} (black solid circle) as a function of total DTPA concentration at I = 0.1 M (Na,H)Cl, T = 25 °C, pcH = 1.42, and $C_{HDEHP} = 7 \times 10^{-2}$ M in TPH.

complexes in aqueous phase with increasing ligand concentration. The slope of the logarithmic variations of D versus the ligand concentration confirms the 1:1 metal−ligand stoichiom-

Table 4. Thermodynamic Parameters Relative to Complexation of Cm(III) with DTPA in (Na,H)Cl Media and (Na,H)ClO_4

complex	ΔG (kJ·mol^{-1})	ΔH (kJ·mol^{-1})	ΔS (J·mol^{-1}·K^{-1})	method	I(M)
$CmHDTPA^-$	−146 ± 2	− 38 ± 13	389 ± 40	TRLFS	0.1
$CmDTPA^{2-}$	−131 ± 2		368 ± 40	TRLFS	0.1
$AmDTPA^{2-}$	−120.6 ± 0.3[a]	−39.5 ± 1[a]	272 ± 40[a]	calorimetry[a]	0.5[a] ($NaClO_4$)

[a]Rizkalla et al.[21]

dx.doi.org/10.1021/ic3011019 | Inorg. Chem. 2012, 51, 12638−12649

etry in the complex. Thus, Am and Cf form complexes of stoichiometry (1,1) with DTPA.

Conditional stability of these complexes was determined by linear fitting of the variations of $(D/D_0 - 1)$ versus C_{DTPA} (where D_0 stands for the D value without DTPA). This leads to lg β^{cond} = 2.7 ± 0.2 for Am and lg β^{cond} = 3.7 ± 0.2 for Cf. Assuming that the protonated species are predominant (pcH = 1.42), the apparent formation constant of protonated complexes $AmHDTPA^-$ and $CfHDTPA^-$ were calculated according to eqs 5 and 8, leading to 25.4 ± 0.4 and 26.5 ± 0.4, respectively, for Am and Cf.

UV−vis spectrophotometry measurements have been performed on Am(III) at pcH = 1.4. Assuming that the predominant species is $AmHDTPA^-$ by analogy with Cm(III), the apparent formation constant lg $\beta_{0,1}$ was equal to 25.9 ± 0.3. A detailed description of this study is provided in the Supporting Information.

3.3.2. CE-ICP-MS. The coupling between the electrophoresis capillary and the mass spectrometer (ICP-MS) allows experiments with Am, Cm, and Cf to be performed simultaneously. The expected slight differences in the formation constants can therefore be regarded as significant and reliable.

Electropherograms were recorded for solutions of pcH 1.42 and 1.92 containing simultaneously the three actinides Am, Cm, and Cf. Figure 5 shows the variation of the peak positions

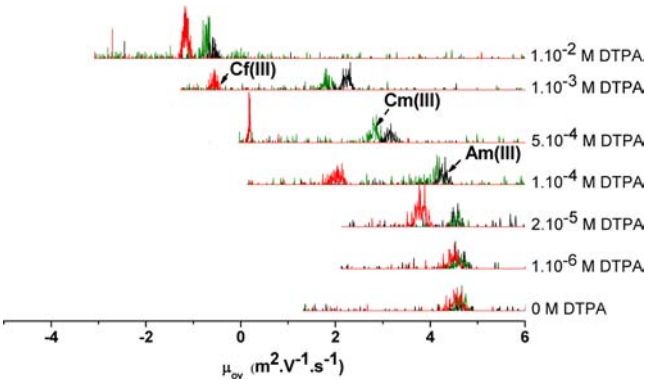

Figure 5. Electropherograms of Cf(III) (red), Cm(III) (green), and Am(III) (black) in 0.1 M (Na,H)Cl, pcH 1.42, T = 25 °C at various DTPA concentrations.

as a function of the overall electrophoretic μ_{ov} and the concentration of DTPA. μ_{ov} varies from positive values to negative ones as DTPA increases. Whatever the DTPA concentration, a single peak is observed for each actinide, which means that molecular exchanges between the different species are faster than the CE migration time.[39] Under such conditions, the species are not separated, and the equilibrium is verified at every elementary stage of the electromigration. Thus, peak positions provide the overall electrophoretic mobility μ_{ov} that depends on the repartition between each species as[27,40]

$$\mu_{ov} = \Sigma_j(x_j \cdot \mu_j) \tag{19a}$$

where x_j and μ_j are the molar fraction and the individual electrophoretic mobility of each metal species, respectively. Development of eq 19 using equilibrium 4 leads to the following expression of the overall electrophoretic mobility

$$\mu_{ov} = \frac{\mu_{An^{3+}} + \beta^{cond} \cdot C_{DTPA} \cdot \mu_{An(III)/DTPA}}{1 + \beta^{cond} \cdot C_{DTPA}} \tag{20}$$

where $\mu_{An^{3+}}$ and $\mu_{An(III)/DTPA}$ stand for the electrophoretic mobility of An^{3+} and An(III)/DTPA complexes, respectively. It can be noticed that eq 20 is then comparable to eq 11 used for analysis of TRLFS data.

Figure 6 illustrates the variations of the overall mobility (μ_{ov}) as a function of the total concentration of DTPA for the three

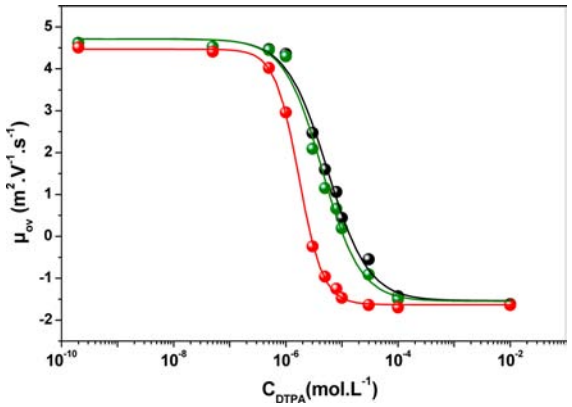

Figure 6. Overall electrophoresis mobility of An(III) (Cf(III), red; Cm(III), green; Am(III), black) species as function of C_{DTPA} in 0.1 M (Na,H)Cl media at 25 °C and pcH = 1.92. Experimental data are symbolized with solid circles and fitting of theoretical expression with line.

actinides studied. The variations of μ_{ov}, from positive to negative values, indicate the transition from a cationic species (An^{3+}) to an anionic species (complex An(III)/DTPA). For $C_{DTPA} > 10^{-4}$ M and pcH 1.92, μ_{ov} values remain constant, indicating that the complexation is total: the overall mobility can therefore be attributed to An(III)/DTPA complexes, i.e., $AnHDTPA^-$ and $AnDTPA^{2-}$ complexes: ($\mu_{ov} = \mu_{An(III)/DTPA} = x_{AnHDTPA^-} \times \mu_{AnHDTPA^-} + x_{AnDTPA^{2-}} \times \mu_{AnDTPA^{2-}}$). The μ_{ov} values become similar for Cf(III), Cm(III), and Am(III) when the DTPA concentration is 10^{-2} mol·L^{-1} for both pcH values. Because the proportion of the complexes is constant at fixed pcH, it might indicate that the average charge as well as the average size of all An(III) species are similar for each actinide and might be explained by a close $[AnHDTPA^-]/[AnDTPA^{2-}]$ ratio for the three elements.

In the absence of ligand the mobility μ_{ov} can be related to the mobility of the actinide aquo ions and $AnCl^{2+}$ (3.7%). The mobility of the actinide aquo ions was recalculated with Anderko's formula.[41] The mobility of Am^{3+} is similar to that of Cm^{3+} and higher than that of Cf^{3+}. This sequence may be explained by the higher hydrated radius (first two hydration spheres) of Cf (4.72 Å) compared to those of Am and Cm (4.65 Å).[42] The μ_{ov} values then decrease following the order $\mu_{ov}Cf(III)) \gg \mu_{ov}(Cm(III)) > \mu_{ov}(Am(III))$ whatever the DTPA concentration, indicating a stronger interaction of DTPA with Cf(III) than with Cm(III) and Am(III).

The variations of experimental μ_{ov} have been fitted with eq 20 allowing conditional formation constants β^{cond} to be determined. At pcH = 1.42 the values are lg β^{cond} = 2.86 ± 0.07 for Am/DTPA, 2.92 ± 0.15 for Cm/DTPA, and 3.88 ± 0.14 for Cf/DTPA. At this pcH, the predominant complex is expected to be the protonated $AnHDTPA^-$ according to

dx.doi.org/10.1021/ic3011019 | Inorg. Chem. 2012, 51, 12638−12649

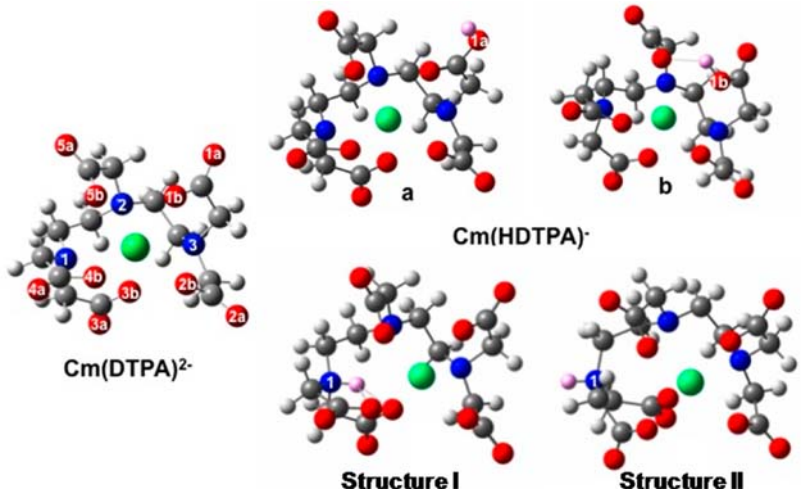

Figure 7. Optimized structures of $Cm(DTPA)^{2-}$ and $Cm(HDTPA)^{-}$ with a proton on oxygen atoms O1a and O1b (structures a and b) or on a nitrogen atom N1 (structures I and II): proton, pink; oxygen atoms, red; nitrogen, blue; carbon, gray; curium, green.

Table 5. Calculated Energy Differences ΔE between the Different Positions of the Proton in the $CmHDTPA^{-}$ Complex[a]

proton position	q_{NBO}	ΔE_{sol}	proton position	q_{NBO}	ΔE_{sol}	proton position	q_{NBO}	ΔE_{sol} (I)	ΔE_{sol} (II)
O1a	−0.71	0	O1b	−0.76	+23	N1	−0.53	+51	+71
O2a	−0.70	+3	O2b	−0.77	+28	N2	−0.54	+65	+106
O3a	−0.70	+10	O3b	−0.78	+48	N3	−0.53	+55	+78
O4a	−0.70	+8	O4b	−0.78	+33				
O5a	−0.71	+5	O5b	−0.76	+29				

[a]Values are in $kJ \cdot mol^{-1}$ and given relative to the lowest energy structure. Electronic atomic charges q_{NBO} in $Cm(DTPA)^{2-}$ obtained from a NBO analysis.

TRLFS results on Cm(III). Then, the apparent formation constants of $AmHDTPA^{-}$, $CmHDTPA^{-}$, and $CfHDTPA^{-}$ have been determined: $\lg \beta_{0.1}$ are 25.5 ± 0.3, 25.6 ± 0.4, and 26.6 ± 0.3 for Am, Cm, and Cf, respectively.

At pcH 1.92, the values of conditional constants relative to Am, Cm, and Cf are 5.23 ± 0.48, 5.32 ± 0.30, and 5.85 ± 0.19. For calculation of apparent formation constants, the $AnDTPA^{2-}$ species must be taken into account. Since $\mu_{An(III)/DTPA}$ was observed to be similar for all An(III) it was assumed that the $[AnHDTPA^{-}]/[AnDTPA^{2-}]$ ratio for the three actinides is identical, and then $\lg K_H = 2.6 \pm 0.6$ (from TRLFS experiments) for Am(III), Cm(III), and Cf(III). Thus, $\lg \beta_{0.0}$ and $\lg \beta_{0.1}$ could be determined (eqs 13−17): 23.1 ± 0.7 and 25.7 ± 0.7 for Am(III), 23.2 ± 0.6 and 25.8 ± 0.6 for Cm(III), and 23.7 ± 0.4 and 26.3 ± 0.4 for Cf(III) (Table 10). The values of $\lg \beta_{0.1}$ obtained for the pcH values seem to be in agreement, which supports our assumption of a similar K_H value for the three elements.

3.4. Structural Investigation. Geometry optimizations at the DFT level were performed in order to compare the coordination geometries of DTPA and HDTPA toward the actinide cations. Full structural investigation was done for Cm^{3+} complexes. The exact number of coordinated water molecules being undetermined, calculations were done with zero, one, and two explicit water molecules around Cm^{3+}. Since the location of the proton in $Cm(HDTPA)^{-}$ complex is also unknown, all protonation sites were considered in the geometry optimizations. Since Am, Cm, and Cf display very close physicochemical properties, calculations relative to Am and Cf have then been performed on the most stable structures obtained with Cm.

In the recent work on europium complexation with DTPA, it was proposed from DFT calculations that the proton in $Eu(HDTPA)^{-}$ complex is located on carboxylate oxygen atoms.[10] However, the calculations were done in the gas phase from the two main starting structures regarding the proton locations.

In order to locate the most likely protonation sites of $Cm(HDTPA)^{-}$ in solution, starting structures were built by locating the proton at all possible sites: the 3 amine nitrogen and 10 carboxylate oxygen atoms (protonation sites are numbered in Figure 7). The proton can be located on an oxygen atom not involved in Cm−HDTPA bonds (oxygens numbered 1a−5a in Figure 7) or an oxygen atom involved in the Cm−HDTPA bonds (oxygen atoms numbered 1b−5b in Figure 7). If nitrogen atoms are protonated, two possible proton arrangements per N were found, as illustrated with structures I and II depicted in Figure 7. Geometry optimizations were performed in solution with an implicit solvent model (through a dielectric continuum model surrounding the complexes). Energy differences between each structure calculated for $Cm(HDTPA)^{-}$ with no water in the complex are reported in Table 5.

The lowest energy structures correspond to structures where the proton is located on the carboxylate oxygen atoms that are not directly involved in the coordination with Cm^{3+}. Complexes b with a proton on the coordinated oxygen atoms are about 20 $kJ \cdot mol^{-1}$ higher in energy than a. Structures with a proton located on the nitrogen atoms are higher in energy. Unexpectedly, structures I where the proton is placed between Cm and N are more stable than structures II (Figure 7). This is due to formation of two hydrogen bonds between H and carboxylate oxygen atoms. The proton preference for the oxygen rather than for the nitrogen atoms is consistent with calculated electronic atomic charges in $Cm(DTPA)^{2-}$ (Table

dx.doi.org/10.1021/ic3011019 | Inorg. Chem. 2012, 51, 12638−12649

5), which are more negative on oxygen than nitrogen by about 0.2 e$^-$. Oxygen "b" are slightly more negatively charged than oxygen "a", while complexes with H on oxygen "a" are lower in energy than those with H on oxygen "b". This is due to strong repulsive interaction between the proton and Cm^{3+} because of the short distance between the two atoms if H is located on the oxygen atoms "b" directly involved in the coordination with Cm^{3+}. The calculated bond distances between Cm and O or N coordinating atoms in $Cm(DTPA)^{2-}$ and $Cm(HDTPA)^-$ are reported in Table 6. In the $Cm(DTPA)^{2-}$ complex, calculated

Table 6. Calculated Cm−O and Cm−N Bond Distances in $Cm(DTPA)^{2-}$ and $Cm(HDTPA)^-$ Complexes (in Angstroms) with H on O1a, O1b, and N1[a]

		Cm(HDTPA)$^-$			
	$Cm(DTPA)^{2-}$	O1a	O1b	N1 structure I	N1 structure II
Cm−O1b	2.42	2.58	2.67	2.34	2.37
Cm−O2b	2.41	2.39	2.37	2.36	2.37
Cm−O3b	2.41	2.36	2.35	2.39	2.32
Cm−O4b	2.39	2.35	2.34	2.47	2.42
Cm−05b	2.42	2.38	2.38	2.39	2.40
Cm−N1	2.74	2.70	2.70	3.51	4.07
Cm−N2	2.66	2.68	2.69	2.79	2.74
Cm−N3	2.70	2.77	2.76	2.63	2.64

[a]See Supporting Information for optimized Cartesian coordinates.

Cm−O distances are about 2.4 Å, while Cm−N distances are 0.3 Å longer (2.7 Å). Upon protonation on an oxygen atom from a carboxylate group, the coordination geometry of the ligand around Cm is only weakly altered, the bond distance between Cm and the O1b atom from the protonated group increases by 0.2 Å, whereas other bond distances slightly vary. Upon protonation of a nitrogen atom, the coordination geometry around the cation is more disturbed by the protonation with a large increase of the Cm−N bond distance involving the protonated nitrogen atom (up to 1.3 Å).

In the presence of one or two water molecules in the inner coordination sphere, several configurations exist which correspond to different arrangements of the water molecules inside the complexes and which are close in energy. Geometry optimizations were done using several starting structures with selected locations of the water molecules and of the proton. The protonation sites considered in the calculation were O1a, O1b, and N1.

With one water molecule, the lowest energy structures are reproduced in Figure 8 and are similar to those found for $Cm(HDTPA)^-$. As obtained for $Cm(HDTPA)^-$, the lowest energy structure corresponds to protonation of one oxygen atom not involved in the Cm−DTPA bonds. Oxygen protonation does not alter much the coordination geometry around the cation.

With two explicit water molecules in complexes ($Cm(DTPA)(H_2O)_2^-$ and $Cm(HDTPA)(H_2O)_2^-$) the inner coordination sphere of the cation is becoming crowded, and geometry optimizations often led to expulsion of one water molecule toward the second coordination shell which becomes hydrogen bonded with carboxylate oxygen atoms. Complexes with only one water molecule coordinating Cm^{3+} and one outside the first shell are lower in energy than those with two water molecules in the inner shell for both DTPA and HDTPA complexes. Besides, protonation of oxygen atoms coordinated

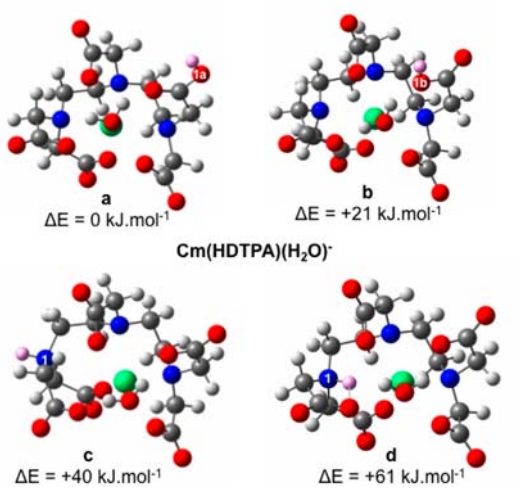

Figure 8. Optimized structures of $Cm(HDTPA)(H_2O)^-$ with a proton on oxygen O1a and O1b (top) or on nitrogen atom N1 (bottom). Calculated energy differences are relative to the structure with H on O1a: proton, pink; oxygen atoms, red; nitrogen, blue; carbon, gray; curium, green.

to curium led to the departure of one carboxylate group away from the curium atoms (Figure 9). However, additional explicit

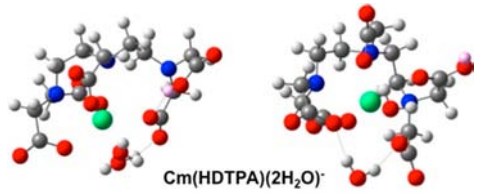

Figure 9. Optimized structures of $Cm(HDTPA)(H_2O)_2^-$ with a proton on oxygen atoms: proton, pink; oxygen atoms, red; nitrogen, blue; carbon, gray; curium, green.

water molecules in the second coordination sphere of the cation are not taken into account in the present model, while they could stabilize the structures with two water molecules in the inner sphere. Molecular dynamics simulations in the presence of a large number of explicit water molecules are out of the scope of the present work but should bring some valuable information on the structure adopted by the complex in the presence of water with DTPA and HDTPA.

To summarize the calculations on $Cm(HDTPA)^-$ and $Cm(HDTPA)(H_2O)^-$, the preferred atomic site for protonation is noncoordinated carboxylate oxygen atoms. Despite protonation, the five carboxylic oxygen and three nitrogen atoms remain coordinated to the cation and the coordination geometry of the ligand around the cation is not strongly disturbed by protonation. This assumption is consistent with the apparent similarity of the fluorescence spectra attributed to $CmDTPA^{2-}$ and $CmHDTPA^-$. Whatever the predominant complex ($CmHDTPA^-$ or $CmDTPA^{2-}$), the measured lifetime was 233 μs. According to the empirical formula of Kimura et al.[43] this lifetime suggests that about two water molecules remain in the inner coordination sphere of Cm(III) in the complex. This is in disagreement with the DFT calculations. Geometry optimizations performed with two explicit water molecules in the complexes indicate that the preferred number of coordinated water molecules is one and that addition of water molecules may lead to the departure of one carboxylate

dx.doi.org/10.1021/ic3011019 | Inorg. Chem. 2012, 51, 12638−12649

function. More information about this discrepancy may be provided by molecular dynamics simulations performed in the presence of a larger number of explicit water molecules, which is out of scope the present work.

Table 7. Calculated Energy Differences between the Different Positions of the Proton and Electronic Atomic Charges in Cm(HDTPA)$(H_2O)^-$ Complex[a]

proton position	ΔE_{sol}	proton position	ΔE_{sol}	proton position	q_{NBO}	ΔE_{sol} (I)*	ΔE_{sol} (II)*
O1a	0	O1b	+23	N1	−0.53	+71	+51
O1b	+21	O2b	+28	N2	−0.54	+106	+65
O3a	+10	O3b	+48	N3	−0.53	+78	+55
O4a	+8	O4b	+33				
O5a	+5	O5b	+29				

[a]Values are in kJ·mol^{-1} and given relative to the lowest energy structure. Electronic atomic charges q_{NBO} in $Cm(DTPA)^{2-}$ obtained from a NBO analysis.

For Am and Cf, structural parameters were calculated for DTPA and HDTPA complexes and with zero and one water molecule. For HDTPA complexes, the proton was located on oxygen atom numbered O1a. Results are given in Tables 8 and

Table 8. Calculated DFT Values of An−O and An−N Bond Distances in $An(DTPA)^{2-}$ and $An(HDTPA)^-$ (Angstroms)[a]

	$An(DTPA)^{2-}$			$An(HDTPA)^-$		
	Am	Cm	Cf	Am	Cm	Cf
An−O1b				2.59	2.58	2.55
⟨An−O⟩	2.42	2.41	2.37	2.37	2.37	2.33
⟨An−N⟩	2.70	2.70	2.68	2.73	2.72	2.69

[a]In $An(HDTPA)^-$, H is located on oxygen atom numbered O1a. ⟨An−N⟩ and ⟨An−O⟩ correspond to the mean values of the distances between An and coordinated nitrogen and oxygen atoms from unprotonated carboxylic functions. See Supporting Information for optimized Cartesian coordinates.

Table 9. Calculated DFT Values of An−O and An−N Bond Distances (Angstroms) in $An(DTPA)(H_2O)^{2-}$ and $An(DTPA)(H_2O)^-$[a]

	$An(DTPA)(H_2O)^{2-}$			$An(HDTPA)(H_2O)^-$		
	Am	Cm	Cf	Am	Cm	Cf
An−O1b				2.63	2.61	2.58
An−O(H_2O)	2.56	2.57	2.52	2.61	2.59	2.57
⟨An−O⟩	2.44	2.43	2.39	2.40	2.40	2.36
⟨An−N⟩	2.79	2.79	2.76	2.78	2.77	2.72

[a]In $An(HDTPA)(H_2O)^-$, H is located on oxygen atom numbered O1a. ⟨An−O⟩ and ⟨An−N⟩ correspond to the mean values of the distances between An and coordinated nitrogen and oxygen atoms from unprotonated carboxylic functions.

9. For all the considered complexes, the coordination geometries around the cation remain similar to those described for Cm. As expected from the diminution of the ionic radii in the series, the bond distances between An and O or N DTPA coordinating atoms decrease from Am to Cf. However, the average distance between An and carboxylic oxygen atoms decreases by 0.04 Å from Cm to Cf, whereas from Am to Cm the decrease does not exceed 0.01 Å. The diminution of 0.04 Å is found in all DTPA and HDTPA complexes, with or without water molecules.

3.5. Discussion. The apparent constants obtained with different techniques in the present work as well as data from previous studies are listed in Table 10. It has to be noted that Baybarz[5] did not consider the protonated complex.

Bayat[23] and Lebedev et al.[17] used the acidity constants from pKa_1 to pKa_5 of ref 7 and neglected pKa_7 and pKa_6 in calculation of apparent formation constants, but their experiments were performed in acidic medium (Table 10). At pcH 1.1, neglecting the two last acidity constants leads to a deviation of −1 on $\lg \beta_{0,n}$ values, whereas the deviation becomes lower than −0.01 at pcH 2.75. The slight difference between the values proposed in the two works might be explained by the difference in pcH range: 1.02 < pcH < 2.42 for Lebedev et al.[17] and higher than 1.82 for Bayat.[23] Neglecting pKa_7 and pKa_6 in the pcH range in the work of Lebedev et al.[17] leads to an underestimate of the values of $\alpha_{HiDTPA^{(5-i)-}}$ used in calculation of apparent formation constants (eq 5), whereas in the pcH range of Bayat's[23] work the dependence of the $\alpha_{HiDTPA^{(5-i)-}}$ values on the two last acidity constants are not very significant.

In the present work, pKa_6 and pKa_7 have been taken into account; nevertheless, our values of $\lg \beta_{0,n}$ are slightly lower than the ones of Bayat.[23] In the present work, the acidity constants from pKa_1 to pKa_3 at 25 °C have been calculated from the values available at 20 °C, whereas Bayat[23] used the values of Moeller and Thompson[7] at 20 °C without any correction. Thus, the value of $\lg \alpha_{DTPA^{5-}}$ was overestimated of 0.15.

These two examples show that the deviation observed in the literature on thermodynamic data relative to An(III)/DTPA complexes might be partly explained by differences in the treatment of auxiliary data on DTPA. Using the same data set and methodology, formation constants of Cm/DTPA and Am/DTPA (Figures S1 and S4, Supporting Information) complexes available in the literature and determined in this work are coherent, whatever the experimental technique (Table 10, Figure 2).

The variation of the apparent formation constants along the trivalent actinides series has only been investigated by Brandau[6] and Baybarz,[5] showing an opposite trend. On one hand, Brandau[8] has shown that the formation constants increase with decreasing metal ionic radius, which indicates that interactions between An(III) and DTPA are mainly ionic. On the other hand, Baybarz[5] observed that stability constants increase from Am^{3+} to Cm^{3+} and decrease from Cm^{3+} to Bk^{3+}. Unfortunately, data on Es and Fm are not reliable. In our work, CE-ICP-MS results, supported by data from solvent extraction (Am, Cf), UV−vis spectrophotometry (Am), and TRLFS (Cm) experiments show clearly the continuous increase of the formation constant from Am to Cf. CE-ICP-MS experiments, in particular, give the opportunity to study simultaneously the three actinides and therefore to deduce a reliable trend. Experimental results are consistent with DFT calculations that indicate a decrease of An−O distance from Am to Cf, the gap being more pronounced between Am and Cf than between Am and Cm. The interaction between An(III) and DTPA is therefore mainly ionic, the ionic character being favored by the five oxygen atoms of carboxylic groups that are hard donors in the sense of HSAB theory.

dx.doi.org/10.1021/ic3011019 | Inorg. Chem. 2012, 51, 12638−12649

Table 10. Apparent Formation Constants of Protonated and Deprotonated Complexes An(III)/DTPA at 25 °C

method	pcH	actinides	$\lg \beta_{0,0}$	$\lg \beta_{0,1}$	$\lg K_H$	media	ref
TRLFS	1.42−2.72	Cm^{3+}	23.0 ± 0.3	25.6 ± 0.3	2.6	(Na,H)Cl 0.1 M	this work
CE-ICP-MS	1.42, 2.72	Am^{3+}	23.1 ± 0.7	25.6 ± 0.7	2.5	(Na,H)Cl 0.1 M	this work
		Cm^{3+}	23.2 ± 0.7	25.7 ± 0.7	2.5		
		Cf^{3+}	23.7 ± 0.4	26.4 ± 0.4	2.5		
spectrometry UV−vis	1.32	Am^{3+}		25.9 ± 0.3		(Na,H)Cl 0.1 M	this work
solvent extraction	1.42	Am^{3+}		25.4 ± 0.4		(Na,H)Cl 0.1 M	this work
		Cf^{3+}		26.6 ± 0.4			
electromigration	1.02−2.42	Am^{3+}	22.74	24.88	2.14	$(K,H)NO_3$ 0.1 M	17
		Cm^{3+}	22.83	24.93	2.1		
ion exchange	1.72−2.92	Am^{3+}	23.07	24.64 ± 0.03	1.6	$(NH_4,H)ClO_4$ 0.1 M	23
	1.82−2.82	Cm^{3+}	23.48	25.01 ± 0.25	1.5		
ion exchange	2.08−2.68	Am^{3+}	22.92	not considered		$(NH_4,H)ClO_4$ 0.1 M	5
		Cm^{3+}	22.99				
		Cf^{3+}	22.57				
solvent extraction	1.72−2.42	Am^{3+}	23.32	26.04	2.72	$(NH_4,H)ClO_4$ 0.1 M	6
		Cm^{3+}	23.81	26.06	2.25		
		Cf^{3+}	24.95	26.47	1.52		

4. CONCLUSION

Complexation of Am, Cm, and Cf with DTPA has been investigated using different experimental techniques, especially CE-ICP-MS, that allowed the three elements to be studied simultaneously in mixture, which ensures the minimization of uncertainties on relative formation constants. The predominant complex was proved to depend on the pcH, and conditional formation constants of $AnHDTPA^-$ and $AnDTPA^{2-}$ have been determined at 25 °C and 0.1 M ionic strength. The affinity of trivalent actinides toward DTPA follows the sequence Cf > Am ≈ Cm for both types of complexes. From TRLFS measurements at different temperatures, complexation reactions were concluded to be exothermic with a high entropic contribution due to disruption of the hydration sphere of the cation and ligand. Systematic DFT calculations on the $CmHDTPA^-$ complex reveal that protonation on a noncoordinated oxygen of the carboxylate group is involved in the most stable structure. Moreover, structures with two water molecules in the inner coordination sphere have been found unstable, indicating that Cm(III) is nine coordinated. In the series Am, Cm, and Cf, for $AnHDTPA^-$ and $AnDTPA^{2-}$ complexes, the distances calculated between the actinide and the donor atoms of DTPA are similar for Am and Cm (within 0.01 Å) while they are shorter for Cf. This follows the trend in formation constants.

■ ASSOCIATED CONTENT

Ⓢ Supporting Information

Experimental details about the preparation of samples, spectrophotometric data on Am/DTPA system and optimized cartesian coordinates of An(III)/DTPA complexes.. This material is available free of charge via the Internet at http://pubs.acs.org.

■ AUTHOR INFORMATION

Corresponding Author

*E-mail: lenaour@ipno.in2p3.fr.

Notes

The authors declare no competing financial interest.

■ REFERENCES

(1) Anderegg, G.; Arnaud-Neu, F; DelgadoFelcman, J.; Popov, K. *Pure Appl. Chem.* **2005**, *77* (8), 1445.
(2) Nilsson, M.; Nash, K. L. *Solvent Extr. Ion Exch.* **2007**, *25*, 665.
(3) Weaper, B.; Kappelman F. A. Talspeak: a new method of separating Americium and Curium from the Lanthanides by extraction from an aqueous solution of an aminopolyacetic acid complex with a monoacidic organophosphate or phosphonate. Report ORNL-3559; Oak Ridge National Laboratory: Oakridge, TN, 1964.
(4) Hérès, X.; Sorel, C.; Miguirditchian, M.; Cames, B.; Hill, C.; Bisel, I.; Espinoux, D.; Eysseric, C.; Baron, P.; Lorrain, B. Results of recent counter-current tests on An(III)/Ln(III) separation using TODGA extractant. *Proceedings of GLOBAL 2009*; CD-ROM SFEN, French Nuclear Energy Society, Paris, France, Sept 6−11, 2009; p 9384.
(5) Baybarz, R. D. *J. Inorg. Nucl. Chem.* **1965**, *27*, 1831.
(6) Brandau, E. *Inorg. Nucl. Chem. Let.* **1971**, *7*, 1177.
(7) Moeller, T.; Thompson, L. C. *J. Inorg. Nucl. Chem.* **1962**, *24*, 499.
(8) Harder, R.; Chaberek, S. *J. Inorg. Nucl. Chem.* **1958**, *11*, 197.
(9) Martell, A. E.; Smith, R. M. *NIST Standard Reference Database 46, Critically Selected stability constants of metal complexes Database*, version 8.0; U.S. Department of Commerce: Washington, DC, 2004.
(10) Tian, G.; Martin, L. R.; Zhang, Z.; Rao, L. *Inorg. Chem.* **2011**, *50*, 3087.
(11) Jezowska-Trzebiatowska, B.; Latos-Grazynski, L.; Kovlowski, H. *Inorg. Chim. Acta* **1977**, *21*, 145.
(12) Latos-Grazynski, L.; Jezowska-Trzebiatowska, B. *J. Coord. Chem.* **1980**, *10*, 159.
(13) Jenkins, B. G.; Lauffer, R. B. *Inorg. Chem.* **1988**, *27*, 4730.
(14) Aime, S.; Botte, M. *Inorg. Chim. Acta* **1990**, *177*, 101.
(15) Benazeth, S.; Purans, J.; Chalbot, M.-C.; Nguyen-Van-Duong., M. M.; Nicolas., L.; Keller, F.; Gaudemer, A. *Inorg. Chem.* **1998**, *37*, 3667.
(16) Delle Site, A.; Baybarz, R. D. *J. Inorg. Nucl. Chem.* **1969**, *31*, 2201.
(17) Lebedev, I. A.; Filimonov, V. T.; Shalinets, A. B.; Yakovlev, G. N. *Sov. Radiochem.* **1968**, *10*, 94.
(18) Moskvin, A. I. *Sov. Radiochem.* **1971**, *13*, 592.
(19) Piskunov, E. M.; Rykov, A. G. *Sov. Radiochem.* **1972**, *14*, 660.
(20) Piskunov, E. M.; Rykov, A. G. *Sov. Radiochem.* **1972**, *14*, 656.
(21) Rizkalla, E. N.; Sullivan, J. C.; Choppin G. R. *Inorg. Chem.* **1989**, *28*, 909.
(22) Choppin, G. R.; Thakur, P.; Mathur, J. N. *Coord. Chem. Rev.* **2006**, *250*, 936.
(23) Bayat, I. *Uber Komplexe dreiwertiger Transurane mit Amino-polykarbonsaüren. KFK Berichte-1291, Karlsruhe*, 1970.
(24) Choppin, G. R.; Thakur, P.; Mathur, J. N. *C. R. Chim.* **2007**, *10*, 916.
(25) Capone, S.; Robertis, A. D.; Stefano, C. D.; Sammartano, S.; Scarcella, R. *Talanta* **1987**, *34*, 593.

(26) Vercouter, T.; Vitorge, P.; Amekraz, B.; Giffaut, E.; Hubert, S.; Moulin, C. *Inorg. Chem.* **2005**, *44*, 5833.
(27) Topin, S.; Aupiais, J.; Baglan, N.; Vercouter, T.; Vitorge, P.; Moisy., P. *Anal. Chem.* **2009**, *81*, 5354.
(28) Frisch, M. J.; Trucks, G. W.; Schlegel, H. B.; Scuseria, G. E.; Robb, M. A.; Cheeseman, J. R.; Montgomery, J. A., Jr.; Vreven, T.; Kudin, K. N.; Burant, J. C.; Millam, J. M.; Iyengar, S. S.; Tomasi, J.; Barone, V.; Mennucci, B.; Cossi, M.; Scalmani, G.; Rega, N.; Petersson, G. A.; Nakatsuji, H.; Hada, M.; Ehara, M.; Toyota, K.; Fukuda, R.; Hasegawa, J.; Ishida, M.; Nakajima, T.; Honda, Y.; Kitao, O.; Nakai, H.; Klene, M.; Li, X.; Knox, J. E.; Hratchian, H. P.; Cross, J. B.; Bakken, V.; Adamo, C.; Jaramillo, J.; Gomperts, R.; Stratmann, R. E.; Yazyev, O.; Austin, A. J.; Cammi, R.; Pomelli, C.; Ochterski, J. W.; Ayala, P. Y.; Morokuma, K.; Voth, G. A.; Salvador, P.; Dannenberg, J. J.; Zakrzewski, V. G.; Dapprich, S.; Daniels, A. D.; Strain, M. C.; Farkas, O.; Malick, D. K.; Rabuck, A. D.; Raghavachari, K.; Foresman, J. B.; Ortiz, J. V.; Cui, Q.; Baboul, A. G.; Clifford, S.; Cioslowski, J.; Stefanov, B. B.; Liu, G.; Liashenko, A.; Piskorz, P.; Komaromi, I.; Martin, R. L.; Fox, D. J.; Keith, T.; Al-Laham, M. A.; Peng, C. Y.; Nanayakkara, A.; Challacombe, M.; Gill, P. M. W.; Johnson, B.; Chen, W.; Wong, M. W.; Gonzalez, C.; Pople, J. A. *Gaussian 03*, revision D.02; Gaussian, Inc.: Wallingford, CT, 2004.
(29) Cao, X. Y.; Dolg, M.; Stoll, H. *J. Chem. Phys.* **2003**, *118*, 487.
(30) Becke, A. D. *J. Chem. Phys.* **1993**, *98*, 5648−5652.
(31) Lee, C.; Yang, W.; Parr, R. G. *Phys. Rev. B* **1988**, *37*, 785−789.
(32) Mondry, A.; Straynowich, P. *Polyhedron* **2000**, *19*, 313.
(33) Allard, B.; Banwart, A.; Bruno, J.; Ephrain, J. H.; Grauer, R.; Grenthe, I.; Hadermann, J. In *Modelling in aquatic chemistry*; Grenthe, I.; Puigdomenech, I., Eds.; OECD Publication: Paris, 1997.
(34) Hummel, W.; Anderegg, G.; Rao, L.; Puigdomench, I.; Tochiyama, O. *Chemical Thermodynamics of Compounds and complexes of U, Np, Pu, Am, Tc, Se, Ni and Zr with selected organic ligands*; OECD Elsevier: Amsterdam, 2005.
(35) Mentasti, E.; Pelizzetti, E.; Saini, G. *J. Chem. Soc.; Dalton. Trans.* **1974**, 1944.
(36) Letkeman, P.; Martell, A. E. *Inorg. Chem.* **1979**, *18*, 1284.
(37) Beitz, J. V. *Radiochim. Acta* **1991**, *52*−*3*, 35.
(38) Guillaumont, R. *Update on the Chemical Thermodynamics of Uranium. Neptunium. Plutonium. Americium and Technetium*; OECD ed.; North-Holland: Amsterdam, 2003; Vol. *5*.
(39) Jiang, C.; Armstrong, D. W. *Electrophoresis* **2010**, *31*, 17.
(40) Topin, S.; Aupiais, J.; Moisy, P. *Electrophoresis* **2009**, *30*, 1747.
(41) Anderko, A.; Lencka, M. M. *Ind. Eng. Chem. Res.* **1997**, *36*, 1932.
(42) David, F. H.; Fourest, B. *New J. Chem.* **1997**, *21*, 167.
(43) Kimura, T.; Choppin, G. R. *J. Alloys Compd.* **1994**, *213*, 313.